

Article

# Deoxygenation of Stearic Acid over Cobalt-Based NaX Zeolite Catalysts

James M. Crawford , Courtney S. Smoljan , Jolie Lucero and Moises A. Carreon \*

Department of Chemical & Biological Engineering, Colorado School of Mines, Golden, CO 80401, USA; jrcrawford@mymail.mines.edu (J.M.C.); csmoljan@mymail.mines.edu (C.S.S.); jlucero1@mymail.mines.edu (J.L.)

\* Correspondence: mcarreon@mines.edu; Tel.: +1-303-273-3329

Received: 22 November 2018; Accepted: 20 December 2018; Published: 4 January 2019



**Abstract:** For the production of sustainable biofuels from lipid biomass it is essential to develop non-noble metal catalysts with high conversion and selectivity under inert gas atmospheres. Herein, we report a novel cobalt-based catalyst supported on zeolite NaX via ion-exchange synthesis. The resultant bifunctional cobalt-based NaX zeolite catalyst displayed high conversion of stearic acid to liquid fuels. In addition, the effect of reaction temperature and catalyst loading was studied to evaluate the order of reaction and activation energy. Decarboxylation and decarbonylation were the dominant deoxygenation pathways. Stearic acid was successfully deoxygenated in N<sub>2</sub> atmospheres using Co/NaX catalysts with a conversion as high as 83.7% and a yield to heptadecane up to ~28%. Furthermore, we demonstrate that higher reaction temperatures resulted in competing pathways of decarboxylation and decarbonylation. Finally, the fresh and recycled catalysts were characterized showing modest recyclability with a ~12.5% loss in catalytic activity.

**Keywords:** deoxygenation; fatty acids; cobalt; stearic acid; non-noble metal; nitrogen atmosphere

## 1. Introduction

Fatty acids are readily extracted from non-edible plants [1,2], algae oil [3], and tallow [4]. These abundant compounds make ideal candidates for the production of biofuels and chemicals. Homogeneous base catalysis of fatty acids yields first-generation fatty acid methyl esters (FAME) by transesterification. Unfortunately, FAMEs have a lower energy density, higher cloud and smoke point, and poor cold flow properties compared to conventional fuels limiting their potential as a “drop-in” fuel solution [5]. As a result, many researchers have turned to heterogeneous catalysts for the selective deoxygenation of fatty acids with the aim of producing diesel range alkanes. Two predominant pathways for the production of alkanes are hydrodeoxygenation resulting in the retention of the parent molecule’s carbon number under hydrogen replete atmospheres and decarboxylation which removes one carbon atom as a carboxylate group under hydrogen deplete atmospheres [5].

Aspects of interest in the valorization of fatty acids include (i) one pot continuous conversion of both saturated and unsaturated fatty acids; (ii) employing non-noble metals for cheaper catalysts; and (iii) decreasing the cost of reaction conditions by lowering temperature/pressure and eliminating hydrogen [6]. With respect to (i), it has been shown that a higher degree of unsaturation in the feedstock results in lower conversion and selectivity [7–9]. Regarding (ii), lower selectivities to alkanes have been shown when removing Pt or Pd from the catalyst [10,11]. Finally, (iii) has proven challenging as hydrogen is required for the saturation of unsaturated fatty acids, leading to attempts to produce in-situ hydrogen from solvents or from sacrificial reactions [11,12]. Recent work has attempted to tackle these concerns by introducing bifunctional catalysts which provide both hydrogenation activity and solid acid activity [13–18]. Zeolites offer highly desirable properties such as high surface areas, good chemical and thermal stability, and strong acidity as a support material for metals [19].

In addition, zeolites have shown industrial maturity and scalability in petroleum processes giving further practicality to their use [20].

Zeolites can be tuned to have specific acidity controlled by the ratio of silica to alumina (Si/Al). More framework aluminum results in a higher concentration of negative charges and higher acidity. Cobalt can be introduced to zeolite supports by ion-exchange synthesis, by which the pore filling agent, in our case, sodium exchanges with the cationic divalent metal in solution. This synthesis method has been applied successfully with cobalt and nickel to a number of zeolites [21,22] and has shown significant benefits when compared to incipient wetness impregnation for the deoxygenation of fatty acids [23].

The zeolite support NaX provides a large surface area, playing an important role in the dispersion of cobalt. Additionally, zeolite NaX is well established as an ideal candidate for ion-exchange due to its large unit cell capacity of approximately 86 cations [24]. Brønsted and Lewis acidity in ion-exchanged NaX zeolites have been well studied [25–27]. In a recent study focusing on monovalent and divalent ion-exchange in NaX it was shown that the intrinsic Brønsted acidity of the zeolite (160  $\mu\text{mol/g}$ ) decreased as the degree of divalent exchange increased. The NaX reached and maintained a minimum Brønsted acidity of approximately 25–40  $\mu\text{mol/g}$  after the divalent ion had replaced over 60% of the  $\text{Na}^+$  [27]. This residual Brønsted acidity coupled with presence of metallic acid sites is hypothesized to provide bifunctionality in our catalyst system. Our group [28,29] and independent groups [30,31] have observed that acidic supports enhance metal dispersion resulting in improved catalytic activity for decarboxylation and hydrodeoxygenation reactions. The catalytic ability of Co based catalysts for hydrodeoxygenation and decarboxylation reactions has been documented [32–36]. For example, Centeno et al. reported the use of Co-noble metal based catalysts for the hydrodeoxygenation reaction of different model molecules containing carbonyl, carboxyl, hydroxyl and methoxy groups [33]. The authors found that the presence of Co favored the decarboxylation activity. A synergistic effect between Co and a noble metal was responsible for this catalytic behavior. Wang et al. attributed also a positive synergistic effect when Co was incorporated into Mo based catalysts leading to an enhanced catalytic activity for hydrodeoxygenation of bio-oils [32]. Furthermore, it has been reported that cobalt-based catalysts can enhance the  $\text{C}(\text{sp}^2)\text{-O}$  cleavage via direct deoxygenation pathway [34]. Zhang et al. found that Co promoted by  $\text{MoS}_2$  favored hydrodecarbonylation yielding more alkene products compared to linear alkanes [36]. Herein, we report a bifunctional cobalt based zeolite NaX (denoted as Co/NaX) supported catalyst implemented under mild reaction conditions and an inert reaction atmosphere yielding high conversion and modest selectivity to heptadecane.

## 2. Results

### 2.1. Nitrogen Physisorption Isotherms

Nitrogen isotherms were collected to estimate surface area, pore volumes, and pore diameters of the parent zeolite NaX, the fresh Co/NaX, and recycled Co/NaX catalysts after use in the deoxygenation reaction (Figure 1). The BET [31] surface area of the NaX zeolite was 788  $\text{m}^2/\text{g}$  in close agreement with previous literature [37]. The BET surface area of Co/NaX and recycled Co/NaX were 447 and 391  $\text{m}^2/\text{g}$ , respectively (Table 1). A clear trend is the reduction in the low pressure uptake of nitrogen, correlated to the surface area, due to the incorporation of cobalt in the zeolites under the alkaline synthesis conditions. Other researchers have seen a similar trend, with a loss in microporous surface area due to metal incorporation in basic synthesis solutions [38,39]. The Co/NaX suffers a 13% loss in surface area after one reaction with stearic acid, which could be tentatively attributed to surface carbon coking the active sites [40]. The Co/NaX also exhibited a  $\sim 13\%$  loss in total pore volume after one reaction. Another important trend is the appearance of mesoporosity after the alkaline synthesis of Co/NaX. Under alkaline synthesis conditions ( $\text{pH} = 8$ ) in low Si/Al zeolites, desilication and mesopore formation has been shown to occur [41]. Mesopore formation may also be attributed to the incorporation of the divalent  $\text{Co}^{2+}$  cation in exchange for monovalent  $\text{Na}^+$ , which could result in

framework alteration [27,42,43]. By introducing mesoporosity in the catalyst, diffusion pathways of large fatty acid molecules are likely less inhibited, giving an argument for the compromise of high surface area.

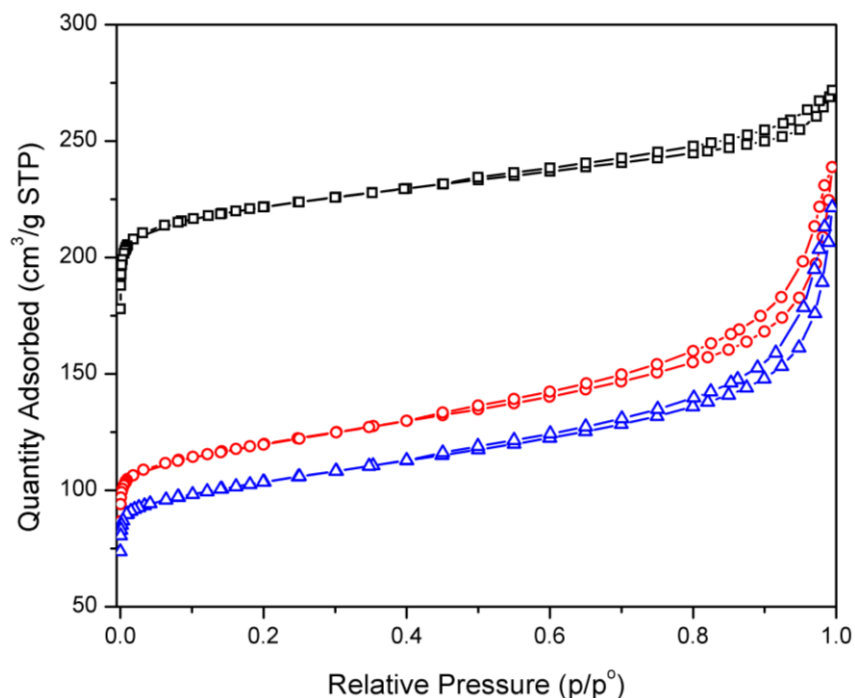


**Figure 1.** Nitrogen isotherms collected at 77 K of the (□) parent NaX zeolite, (○) Co/NaX, (△) and recycled Co/NaX.

**Table 1.** Physical properties of the parent zeolite and the fresh and recycled Co/NaX catalyst.

| Catalyst        | Surface Area [ $\text{m}^2 \cdot \text{g}^{-1}$ ] |             | Pore volume [ $\text{cm}^3 \cdot \text{g}^{-1}$ ] |               |              |              |
|-----------------|---|-------------|---|---------------|--------------|--------------|
|                 | $S_{BET}$   | $S_{ext}^1$ | $V_{tot}^2$                                       | $V_{micro}^1$ | $V_{meso}^3$ | $V_{meso}^4$ |
| NaX             | 788   | 106         | 0.40  | 0.28          | 0.12         | 0.15         |
| Co/NaX          | 447   | 117         | 0.31  | 0.12          | 0.19         | 0.25         |
| Recycled Co/NaX | 391   | 108         | 0.27  | 0.10          | 0.18         | 0.23         |

<sup>1</sup> External surface area and micropore volume were calculated by the *t*-plot method, <sup>2</sup> total volume was calculated from the quantity adsorbed at  $P/P^0 = 0.975$ , <sup>3</sup> mesopore volume = total volume – micropore volume, <sup>4</sup> mesopore volume was calculated by BJH method.

Pore diameter was evaluated using BJH method on the desorption branch of the isotherm (Figure 2). A high nitrogen uptake at  $\sim 15 \text{ \AA}$  is highly pronounced in the parent NaX zeolite in good agreement with previous literature [37]. This uptake reduces in the Co/NaX and recycled samples, indicating fewer micropores. A secondary peak at  $45 \text{ \AA}$  shows increasing intensity in the Co/NaX and recycled samples, correlating well with the increase in mesoporosity.

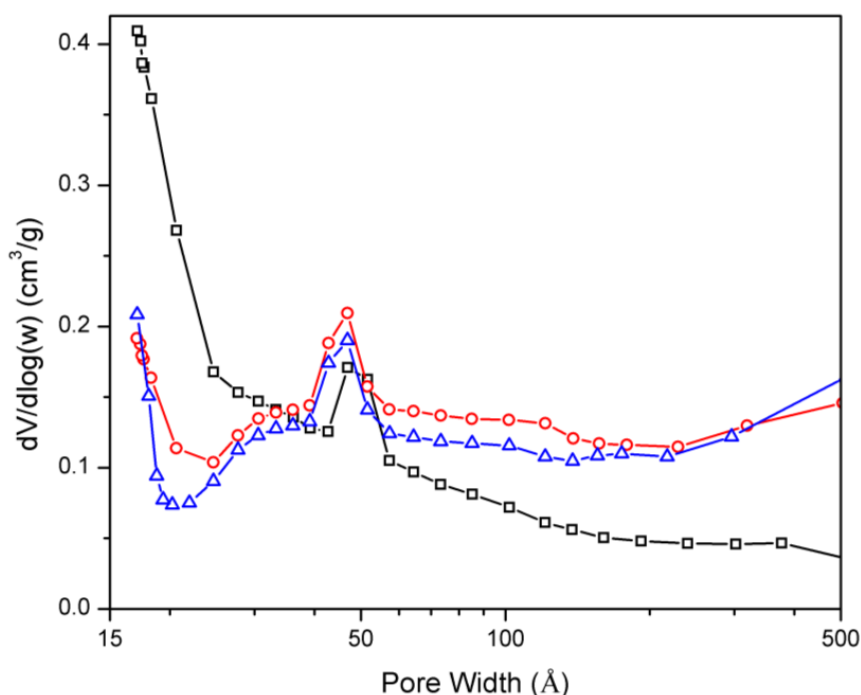


**Figure 2.** BJH pore size distribution of the (□) parent NaX zeolite, (○) Co/NaX, (△) and recycled Co/NaX.

## 2.2. Powder X-Ray Diffraction

The synthesized NaX zeolite exhibits high crystallinity matching well with the simulated X-ray diffraction (XRD) pattern (Figure 3). After ion-exchange synthesis with  $\text{Co}(\text{NO}_3)_2$ , calcination, and reduction, the presence of strong  $\text{Co}_3\text{O}_4$  peaks were observed at  $36.49^\circ$  and  $43.20^\circ$  corresponding to (331) and (400) planes, respectively (JCPDS # 76-1802). The cobalt oxide peaks gave a calculated average nanoparticle size of 17.9 and 19.6 nm for the fresh and recycled Co/NaX catalysts respectively from the Scherrer equation ( $d_{\text{avg}} = K\lambda/\omega\cos\theta$ , where  $d_{\text{avg}}$  is the estimated average particle size,  $K = 0.9$  is the shape factor,  $\lambda = 1.5406 \text{ \AA}$  is the Cu  $K\alpha$  radiation,  $\omega$  is the full width of the half maximum intensity, and  $\theta$  is the Bragg angle). The increase in nanoparticle size may be due to sintering of metallic species during the regeneration steps. The strong cobalt oxide peak is characteristic of high cobalt loadings in the pore of the zeolite. It should be noted that complete reduction of the sample was not achieved at the conditions employed. Use of higher reduction temperatures would promote metallic species formation, but may also result in larger particle agglomeration [44].

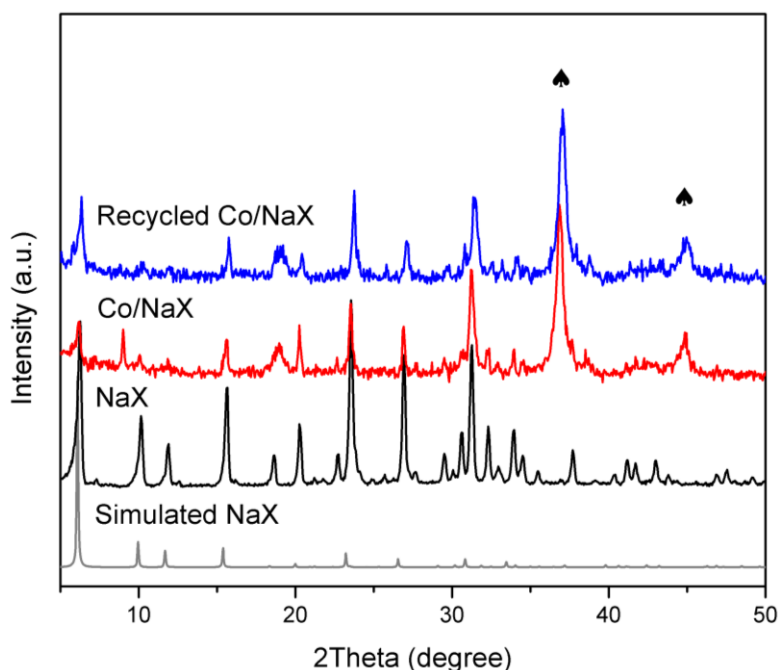


**Figure 3.** Powder XRD of the catalysts. Cobalt oxide peaks are denoted by ♠.

### 2.3. Thermogravimetric Analysis

Catalysts were evaluated for thermal stability by thermogravimetric analysis (TGA) (Figure 4). Weight loss up to 250 °C was attributed to physisorbed water, and loss between 250–700 °C was attributed to carbonaceous coke on the spent sample [45]. Fresh and recycled samples exhibit high thermal stability up to 700 °C. The spent catalyst, after a typical reaction ( $T = 280$  °C, Loading = 250 mg), showed a weight loss of 36% attributed to coke deposited on the surface. High coke contents have been reported in zeolite materials for biomass upgrading and can lead to deactivation of the catalyst [45,46].

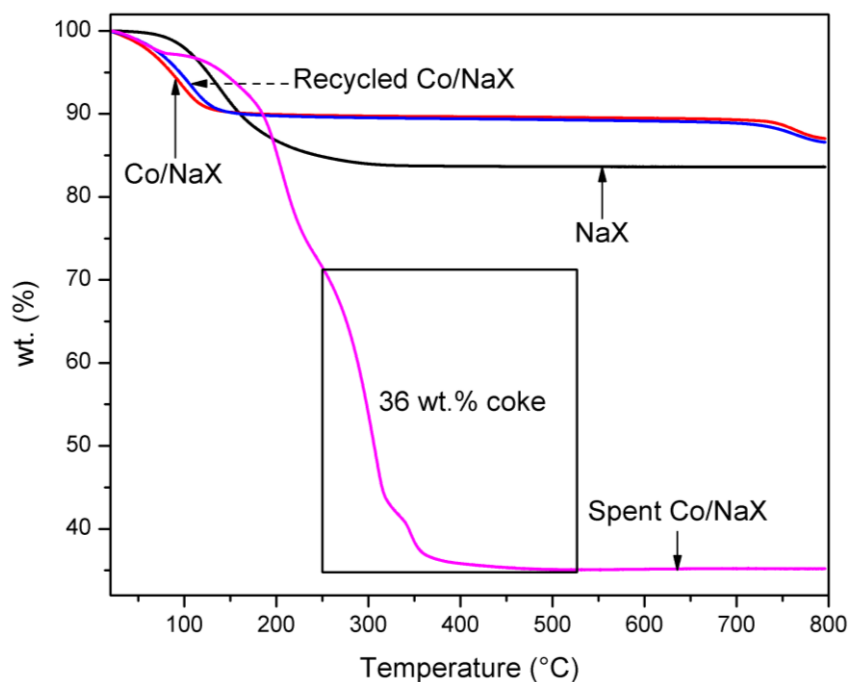


**Figure 4.** TGA of the spent catalyst shows a significant accumulation of coke.

#### 2.4. Attenuated Total Reflectance Fourier Transform Infrared Spectroscopy

For the evaluation of the surface composition of the synthesized catalysts, attenuated total reflectance Fourier transform infrared spectroscopy was employed (ATR-FTIR). ATR-FTIR of ion-exchanged zeolite materials have been modeled and studied by Król et al. [47]. They suggest that the band located at  $560\text{ cm}^{-1}$  is sensitive to the ion-exchange synthesis and acts as an indicator of the sorption process. Shown in Figure 5A, both Co/NaX and recycled catalysts show major increases at the stretch at  $560\text{ cm}^{-1}$ , indicating a successful ion-exchange of  $\text{Na}^+$  for  $\text{Co}^{2+}$ .

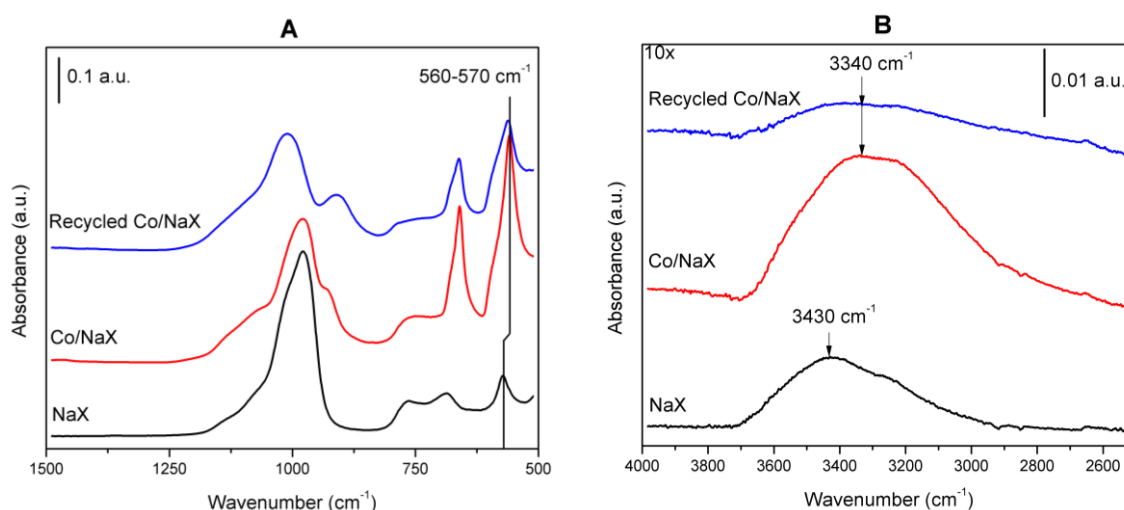


**Figure 5.** ATR-FTIR of the catalysts where (A) a large shift and increasing intensity of the band at  $560\text{ cm}^{-1}$  indicated ion-exchange of Na with Cobalt and (B) loss of the  $3430\text{ cm}^{-1}$  band (10x magnification) could indicate coke coverage of the hydroxyl groups.

Coking on zeolitic materials can be qualitatively observed by ATR-FTIR. Generally, bridging hydroxyl groups are observed in the region between  $3200\text{--}3800\text{ cm}^{-1}$  in zeolites, shifting with a dependence on cavity size, Si/Al ratio, and cation occupancy [48]. The  $\nu(\text{O-H})$  region around  $3430\text{ cm}^{-1}$  has been shown to adopt this position in highly acidic zeolites [49]. Shifting of this peak in the cobalt exchanged catalyst to  $3340\text{ cm}^{-1}$  is hypothesized to be caused by interactions of the hydroxyls with the new metal cation (Figure 5B). The recycled catalysts loss of intensity could indicate graphitic coke coverage on the bridging hydroxyl groups [50]. Coke composition on the catalyst is discussed in Section 3.2.

#### 2.5. Field-Emission Scanning Electron Microscopy

Field-Emission scanning electron micrographs of the parent NaX, the fresh Co/NaX, and the recycled Co/NaX catalyst are shown in Figure 6. A clear morphology shift from smooth octahedral NaX zeolite to a roughened surface containing cobalt is the result of the alkaline synthesis. This is in good agreement with the increase in external surface area calculated from the  $\text{N}_2$ -isotherm. The location of the cobalt species and oxygen species were elucidated by energy-dispersive X-ray spectroscopy (EDX) shown in Figure S1. Clearly, the cobalt was well dispersed across the surface of the zeolite with no major agglomeration. Additionally, the cobalt appeared to be dispersed similarly to the oxygen, silicon, and aluminum, suggesting that the cobalt was located similarly throughout the cavities of the zeolite.

Using EDX quantification, the fresh and recycled Co/NaX cobalt loading was calculated to be similar at  $\sim 23\%$  and  $\sim 26\%$ , respectively (Figure S2). The slightly higher loading in the recycled catalyst was within the experimental error range of EDX. Nevertheless these results indicate that Co leaching was negligible due to the reaction. The Si/Al ratio of the parent NaX, fresh Co/NaX, and recycled Co/NaX was found to be 1.3, 1.6, and 1.5, respectively in close agreement with previously reported ion-exchanged NaX materials [27]. The Na/Al ratio was used to observe the extent of ion-exchange

trending downward from the parent zeolite NaX to the fresh and recycled Co/NaX giving 0.72, 0.23, 0.26, respectively. This trend indicates that the cobalt replaced the sodium in the zeolite cages.

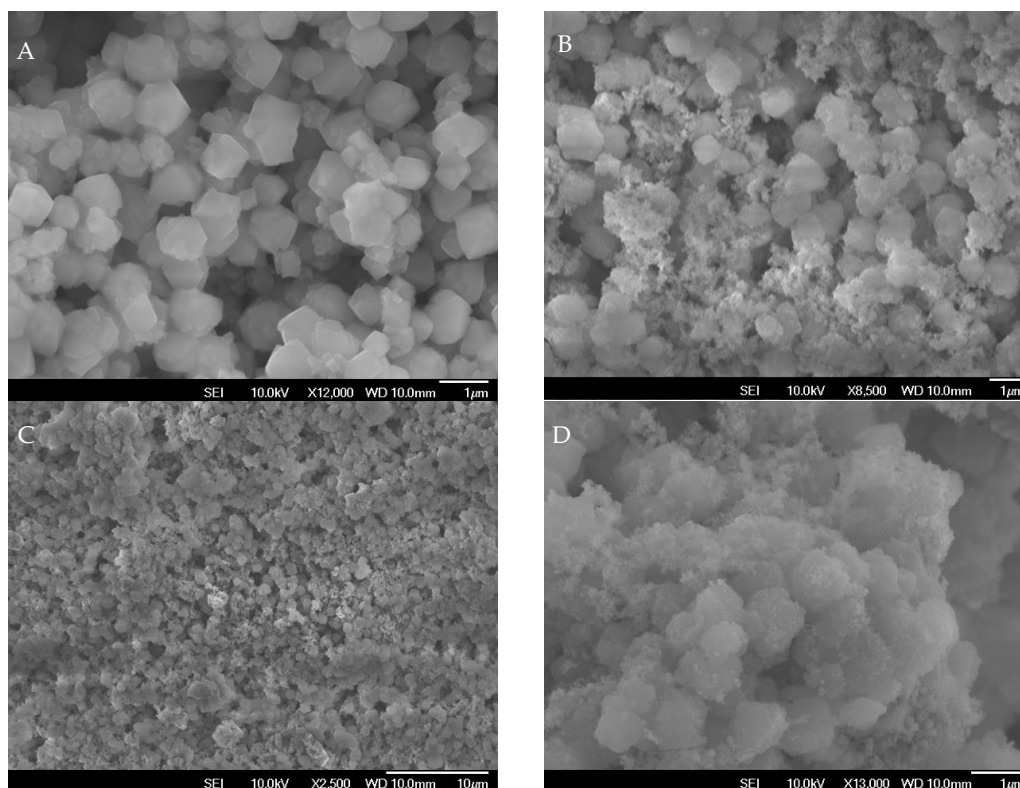


**Figure 6.** Representative SEM micrographs of (A) synthesized NaX zeolite, (B) fresh Co/NaX, (C) fresh Co/NaX at a larger scale, (D) recycled Co/NaX.

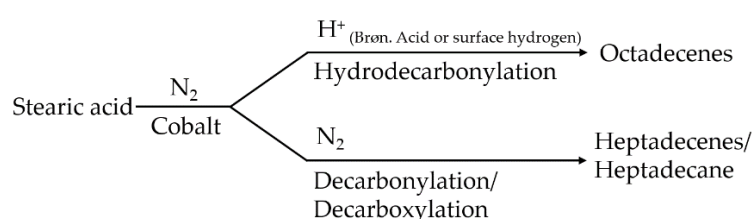
### 2.6. Deoxygenation of Stearic Acid over Co/NaX in N<sub>2</sub>

Deoxygenation of stearic acid was conducted in the presence of nitrogen over Co/NaX catalysts. The reaction temperature was varied between 260–300 °C. Table 2 shows the catalytic performance of the parent zeolite NaX and Co/NaX at various reaction temperatures and catalysts loadings. The conversion correlated to the reaction temperature, with the lowest conversion at 260 °C and the highest conversion at 300 °C. Selectivity to heptadecane (C<sub>17</sub>) was highest at 280 °C. Yield to C<sub>17</sub> was highest at 280 °C followed closely by 300 °C giving 27.9 and 25.7%, respectively. The reaction conducted at 280 °C was repeated to ensure reproducibility. Two major reaction pathways for the Co/NaX catalyst included decarboxylation and decarbonylation evidenced by the dominant formation of C<sub>17</sub> and C<sub>17</sub>-ene products. Similar results were found by Zhang et al. showing selectivity losses to alkene products [36]. Additionally, some octadecene was observed, a result of the hydrodecarbonylation pathway [51]. The formation of octadecene requires the presence of Brønsted acid sites [52], which have been shown to be present in ion-exchanged zeolite NaX [27]. We hypothesize that both the Brønsted acidity of the support and residual surface hydrogen on the reduced Co/NaX catalyst provided protonic H<sup>+</sup> [53] which could have participated in the hydrodecarbonylation reaction. This would also explain the observed formation of the intermediate hydrodecarbonylation species, octadecanol (observed in the “other” column in Table 2). The proposed pathway is outlined in Scheme 1. Overall, the non-noble metal Co/NaX catalyst provided good conversion and modest selectivity to heptadecane. The catalyst loading had an effect on the selectivity. At low loadings, low conversion was observed, along with very high selectivity to C<sub>17</sub> products. This trend may be due to the relatively high loading of cobalt on the catalyst, which promotes decarbonylation in competition with decarboxylation.

**Table 2.** Product distribution for the deoxygenation of stearic acid over Co/NaX catalyst in N<sub>2</sub>.

| Entry | Catalyst                     | Loading (mg) | Temp. (°C) | $X_{TOT}$ (%) | Product Distribution (%) |                     |                     |       | $Y_{C17}$ (%) |
|-------|------------------------------|--------------|------------|---------------|--------------------------|---------------------|---------------------|-------|---------------|
|       |                              |              |            |               | C <sub>17</sub>          | C <sub>17-ene</sub> | C <sub>18-ene</sub> | Other |               |
| 1     | NaX (blank)                  | 250          | 280        | 23.7          | 21.2                     | 21.7                | 6.5                 | 50.6  | 5.0           |
| 2     | Co/NaX                       | 15           | 280        | 30.9          | 71.0                     | 16.6                | 0.0                 | 12.3  | 22.0          |
| 3     | Co/NaX                       | 150          | 280        | 67.1          | 17.1                     | 30.1                | 36.4                | 16.4  | 11.5          |
| 4     | Co/NaX                       | 250          | 280        | 78.8          | 32.1                     | 30.7                | 9.9                 | 27.3  | 25.3          |
| 5     | Co/NaX                       | 250          | 260        | 54.2          | 27.5                     | 21.1                | 7.3                 | 44.1  | 14.9          |
| 6     | Co/NaX                       | 250          | 280        | 83.7          | 33.3                     | 31.9                | 19.7                | 15.1  | 27.9          |
| 7     | Co/NaX                       | 250          | 300        | 95.1          | 27.0                     | 32.5                | 28.4                | 12.0  | 25.7          |
| 8     | Co/NaX Recycled <sup>1</sup> | 230          | 280        | 70.5          | 21.9                     | 31.7                | 31.8                | 14.6  | 15.4          |

Experimental conditions: Stearic acid (3.51 mmol), n-hexane (10 mL), catalyst (250 mg),  $t = 2$  h,  $P = 10$  bar N<sub>2</sub> (room temperature),  $X_{TOT}$  = conversion,  $Y_{C17}$  = yield to heptadecane. <sup>1</sup> 230 mg of catalyst were recovered from the reactor and were recycled from entry 6, Catalyst:Stearic acid ratio was maintained at 1:4.



**Scheme 1.** Conversion of stearic acid over Co/NaX lead to the formation of hydrodecarbonylation, decarbonylation, and decarboxylation products.

### 3. Discussion

#### 3.1. Effect of Catalyst Loading and Temperature

To better understand the behavior of the Co/NaX catalyst under nitrogen atmosphere, first the loading of the catalyst was varied. When comparing the catalyst loading (15, 150, 250 mg) to a first order rate expression calculated from the stearic acid conversion, a linear relationship was observed ( $R^2 = 0.999$ ), indicating a pseudo-first-order reaction (Figure 7A). Therefore, based on the first-order nature of the disappearance of stearic acid, we calculated the apparent activation energy of the reaction. An Arrhenius plot (Figure 7B) was prepared from the explored reaction temperatures (533, 553, 573 K) with all other reaction conditions held constant. From a linear regression ( $R^2 = 0.9948$ ) the apparent activation energy was calculated to be  $93.5 \pm 0.5$  kJ/mol. This value for the decarboxylation of stearic acid (the most dominant pathway) is in good agreement with values found by other researchers [54–56].

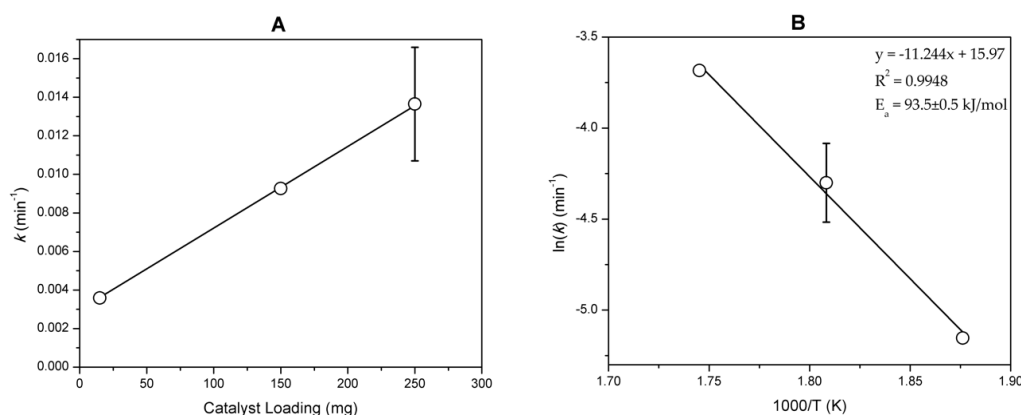


**Figure 7.** Variation of the (A) catalyst loading ( $T = 280$  °C) showing first-order behavior for the disappearance of stearic acid compared to the catalyst loading and the (B) temperature (loading = 250 mg) showing Arrhenius behavior for increasing temperatures. Error bars are the range about the average of the two data points collected at 250 mg catalyst and  $T = 280$  °C.

### 3.2. Catalyst Recyclability

Physically, the catalyst has many desirable properties including thermal stability and maintenance of crystallinity evidenced by the XRD and TGA results. In addition, the catalyst did not exhibit significant metal leaching according to the loading from EDX. However, after calcination and reduction, the catalyst exhibited a loss of catalytic activity. From the TGA analysis, it was apparent that a large amount of coke (36 wt.%) was present on the catalyst. Further analysis of the coke as described by Migliori et al. provided some insight into the species present at the surface [57,58]. The carbonaceous coke was mostly composed of large aromatic species and oxygenates (Table 3). The graphitic compounds likely remained on the active sites even after regeneration [59] contributing to the ~12.5% loss in activity when compared to the fresh catalyst. The ATR-FTIR spectra indicated that carbonaceous coke was likely present on the recycled catalyst surface evidenced by the disappearance of the broad stretch in the 3200–3500 cm<sup>-1</sup> region. Such coke deposits have been widely shown to cause deactivation in heterogeneous catalysts. This is supported by the lower surface area displayed by the recycled catalyst.

**Table 3.** Composition of soluble coke by GC-MS analysis on Co/NaX after a typical reaction.

| Compound   | Area (%) |
|--|----------|
| Aromatic   |          |
| 1H-trindene, 2,3,4,5,6,7,8,9-octahydro-1,1,4,4,9,9-hexamethyl- | 87       |
| Aldehyde   |          |
| benzaldehyde, 3-methyl-  | 10       |
| Phenol   |          |
| oxirane, [[4-(1,1-dimethylethyl)phenoxy]methyl]-               | 2.5      |
| Ketone   |          |
| 2,4,6-cycloheptatrien-1-one                                    | 1.5      |

### 3.3. Comparison of the State-of-the-Art of Cobalt-Based Catalysts

Table 4 compares the state-of-the-art Co-based catalysts for deoxygenation of fatty acids to liquid hydrocarbons. Our catalysts show comparable conversions to previous reports in which hydrogen was employed as the gas atmosphere, and the best performance under inert conditions (nitrogen). Although higher yields have been observed under hydrogen environment, the use of hydrogen in the conversion of fatty acid involves processing safety concerns on scale-up along with potentially negative environmental impacts due to the energy intensity involved in obtaining the gas [60,61]. For these reasons, we believe that the Co/NaX catalysts may contribute in a meaningful way to the advance of biofuel production under inert environments. Nevertheless, more research is needed to improve both the yield to deoxygenation products, and to improve the catalytic stability of Co/NaX catalysts.

**Table 4.** State-of-the-art comparison of Co-based catalysts in the deoxygenation of vegetable oils.

| Ref.      | Catalyst                            | Reactant          | Pathway | Synthesis | Rxn Conditions                        | Major Product        | X <sub>TOT</sub> (%) | Yield (%) |
|-----------|-------------------------------------|-------------------|---------|-----------|---------------------------------------|----------------------|----------------------|-----------|
| [36]      | Co/MoS <sub>2</sub>                 | Canola Oil        | HDO     | Hydro     | 375 °C, 90 bar H <sub>2</sub> , 8 h   | C <sub>17</sub> -ene | 80                   | -         |
| [62]      | Co/HZSM-5                           | Stearic Acid      | HDO     | SOMC      | 260 °C, 30 bar H <sub>2</sub> , 4 h   | C <sub>18</sub>      | 100                  | 80        |
| [63]      | Co/HZ-5                             | Palmitic Acid     | HDO     | SS        | 260 °C, 40 bar H <sub>2</sub> , 4 h   | C <sub>18</sub>      | 100                  | 49.5      |
| [63]      | Co/HZP-5                            | Palmitic Acid     | HDO     | SS        | 260 °C, 40 bar H <sub>2</sub> , 4 h   | C <sub>16</sub>      | 100                  | 47.6      |
| [64]      | Co <sub>2</sub> S/Clay              | Methyl Oleate     | HDO     | WI        | 300 °C, 40 bar H <sub>2</sub> , 6 h   | C <sub>18</sub>      | 100                  | 89        |
| [65]      | Co/γ-Al <sub>2</sub> O <sub>3</sub> | Palm Oil          | HDO     | IW        | 300 °C, 50 bar H <sub>2</sub> , 100 h | C <sub>16</sub>      | 100                  | 35        |
| [66]      | Co/MgO                              | Methyl Heptanoate | HDO     | IW        | 220 °C, 30 bar H <sub>2</sub> , 6 h   | C <sub>7</sub>       | 73.3                 | 1.7       |
| [66]      | Co/SiO <sub>2</sub>                 | Methyl Heptanoate | HDO     | IW        | 220 °C, 30 bar H <sub>2</sub> , 6 h   | C <sub>7</sub>       | 98.3                 | 44.8      |
| [66]      | Co/Hβ                               | Methyl Heptanoate | HDO     | IW        | 220 °C, 30 bar H <sub>2</sub> , 6 h   | C <sub>7</sub>       | 99.7                 | 38.4      |
| [67]      | Co/SBA-15                           | Methyl Oleate     | HDO     | IW        | 340 °C, H <sub>2</sub> , 6 h          | C <sub>17</sub>      | 90                   | 49.5      |
| [16]      | Co(Oac) <sub>2</sub>                | Stearic Acid      | DCO     | No synth  | 350 °C, N <sub>2</sub> , 2 h          | C <sub>17</sub>      | 31                   | 1.5       |
| This work | Co/NaX                              | Stearic Acid      | DCO     | IE        | 280 °C, 10 bar N <sub>2</sub> , 2 h   | C <sub>17</sub>      | 83.7                 | 27.9      |

IW: Incipient wetness impregnation; IE: Ion-exchange; Hydro: Hydrothermal synthesis; SOMC: Surface organometallic grafting chemistry; SS: Solid state impregnation; WI: Wet impregnation.

## 4. Materials and Methods

### 4.1. Materials and Chemicals

Hexane (95%, HPLC, Sigma-Aldrich, St. Louis, MO, USA) and stearic acid (95%, Sigma-Aldrich) were used in the deoxygenation reaction. For the GC analysis, N,O-Bis(trimethylsilyl)trifluoro-acetamide (BTSFA) (99%, GC, Sigma-Aldrich) and n-Hexadecane (95%, Alfa Aesar, Ward Hill, MA, USA) were used as the volatilizing agent and internal standard, respectively. Ethyl alcohol (200 proof pure, Sigma-Aldrich), Petroleum Ether (35/60, Alfa Aesar), Phenolphthalein (1% w/v, Alfa Aesar), and Sodium Hydroxide Solution (0.1N, Sigma-Aldrich) were used in the acid value test. Cobalt (II) Nitrate Hexahydrate (98%, Sigma-Aldrich), Sodium Aluminate (Anhydrous, Sigma-Aldrich), Ludox AS-40 (Colloidal, Sigma-Aldrich), Sodium Hydroxide Pellets (ACS, Sigma-Aldrich), and 28% Ammonia hydroxide solution (Sigma-Aldrich) were used in the synthesis of the NaX zeolite and Co/NaX catalyst. Hydrofluoric acid (HF, 48% in water, Sigma-Aldrich) and methylene chloride (99.8%, Fischer-Scientific, Waltham, MA, USA) were used for coke compositional analysis.

### 4.2. Zeolite NaX Synthesis

Zeolite NaX was synthesized in a molar ratio of  $3.5\text{Na}_2\text{O}:\text{Al}_2\text{O}_3:4\text{SiO}_2$  as described elsewhere [68]. Briefly, a solution of sodium aluminate and an aqueous solution of sodium hydroxide was mixed homogeneously. Then, Ludox AS-40 was added and stirred for 40 min at room temperature. Next, 40 mL of solution was transferred into a 100 mL PTFE lined Parr autoclave and heated to 90 °C for 15 h at 1 °C/min heating and cooling rates. After, the zeolite was washed by centrifugation until the solution was below a pH = 8. The zeolite was then dried overnight at 100 °C and used for the synthesis of Co/NaX.

### 4.3. Co/NaX Ion-Exchange Synthesis

An aqueous solution of distilled water and Cobalt (II) nitrate hexahydrate (0.28 M, 50 mL) was stirred until homogeneous. Next, 5.025 g of zeolite NaX prepared as described above was added to the cobalt nitrate solution and stirred homogeneously. Dropwise addition of 3% ammonia solution was conducted until pH = 8. The solution was covered and stirred at room temperature for 180 min. Finally, the catalyst was collected by vacuum filtration and washing three times with distilled water. The resulting solid was dried overnight at 110 °C, calcined at 450 °C with a 1 °C/min ramp rate, and reduced under 150 mL/min  $\text{H}_2$  at 460 °C with a 1 °C/min ramp rate. After reduction, the obtained Co/NaX was employed as catalyst for the deoxygenation of stearic acid.

### 4.4. Catalyst Characterization

Fresh and recycled catalysts were characterized by the following analyses: Textural properties were evaluated by collecting nitrogen adsorption-desorption isotherms. Prior to these experiments, samples were degassed at 300 °C for 5 h (ASAP 2020 porosimeter, Micromeritics, Norcross, GA, USA). The crystalline phase of the catalysts was determined by XRD (Siemens, Munich, Germany, Kristalloflex800, 25 mA, 30 kV,  $\text{CuK}\alpha$  radiation). FE-SEM images were obtained using a field emission gun and accelerating voltage of 10 kV (JEOL ISM-7000F, Peabody, MA, USA). ATR-FTIR was conducted using 10 scans,  $4\text{ cm}^{-1}$  resolution, DTGS detector (Thermo Scientific Nicolet iS50 FT-IR, Madison, WI, USA). TGA was conducted with at least 10 mg of sample, ramped from room temperature to 800 °C, 10 °C/min, 50 mL/min  $\text{N}_2$ , 50 mL/min air (TA Instruments, New Castle, DE, USA). For coke compositional analysis, methods were adapted from Migliori et al [57]. Briefly, 15 mg of Co/NaX was completely dissolved in 1 mL of 48% hydrofluoric acid after 15 min. Then, 5 mL of methylene chloride was added and mixed for 2 min. Finally, the solution was allowed to separate into the two phases for 1 h. After, 2  $\mu\text{L}$  of the organic phase was sampled for GC-MS, following the procedure outlined in the liquid product analysis.

#### 4.5. Catalytic Reaction: Deoxygenation Experiments

In a typical reaction, 250 mg of Co/NaX catalyst was loaded with 1000 mg of stearic acid in a 100 mL Parr batch reactor. 10 mL of hexane was added and the reactor was sealed. The reactor was then pressurized with nitrogen to 10 bar and flushed three times to remove stagnant air. The reactor was finally pressurized to 10 bar N<sub>2</sub> and sealed. Stirring at 600 rpm was initiated and the reactor was heated rapidly to 280 °C and held for 2 h. The reaction conditions were shown to be in the kinetic regime ( $\eta = 0.99$ , Table S1) [69–71]. The pressure after the heating phase was noted to be ~35 bar on reaching 280 °C and 38 bar after 2 h at 280 °C. After the reaction was complete, the reactor was cooled with forced air until at room temperature. Finally, the chamber was depressurized and the resultant liquid products were sampled. The catalyst was recovered from the liquid products by suspension in 20 mL of hexane and sonicated for 5 min. The sonicated solution was then centrifuged, decanted, and the resultant solid (spent catalyst) was calcined at 400 °C for 4 h, 5 °C/min ramp, and reduced at the same conditions described in Section 4.3. The obtained recycled Co/NaX was then characterized and evaluated for an additional reaction.

#### 4.6. Liquid Product Analysis

Products were weighed and added along with 10  $\mu$ L of BTSFA, 5  $\mu$ L of n-Hexadecane, and 1000  $\mu$ L of hexane into a glass 2 mL vial. The contents were sealed and placed in an oven at 60 °C for 60 min to allow the silylation of the fatty acids. A gas chromatography (Agilent GC, 6980N, Santa Clara, CA, USA) mass spectrometer (Agilent MSD, 5973N) equipped with a HP-5 molecular sieve column (30 m  $\times$  250  $\mu$ m  $\times$  0.25  $\mu$ m) in split mode with carrier gas He (10:1) was used for product detection. The oven program was set to: Ramp 40–300 °C at 10 °C/min, interface: 260 °C, ion source: 250 °C, 2  $\mu$ L injection.

The conversion of stearic acid was calculated by the removal of the carboxylic acid groups by the acid value test (ASTM D5558). The acid value was calculated by Equation (1):

$$AV = \frac{56.1(N)(V_f - V_o)}{w} \quad (1)$$

where  $N$  is the normality of the sodium hydroxide solution,  $w$  is the mass of the sample, and  $V_f$  and  $V_o$  are the initial and final volume of sodium hydroxide. The acid value of stearic acid was found to be 194 in good agreement with literature values. The conversion,  $X_{TOT}$ , of stearic acid was calculated by Equation (2):

$$X_{TOT} = (AV_{SA} - AV_{Prod}) / AV_{SA} * 100 \quad (2)$$

where  $AV_{SA}$  and  $AV_{Prod}$  were the acid value of stearic acid and the products, respectively.

## 5. Conclusions

In summary, we demonstrate that cobalt-based catalysts supported on zeolite NaX displayed catalytic activity for the deoxygenation of stearic acid to heptadecane in the presence of inert environment. The high conversion of the Co/NaX catalyst was attributed to the mesoporosity introduced in the alkaline synthesis shown in the N<sub>2</sub>-isotherm, the bifunctionality of the acidic zeolite support, and the high loading of active Co metal. Heptadecane yields as high as 27.9% were observed at an optimal 280 °C under nitrogen atmospheres through the decarboxylation pathway. The highest conversion, 95%, was observed at the highest explored temperature, 300 °C, with some heptadecane selectivity losses to alkenes. Some hydrodecarbonylation products were observed and were attributed in part to the hypothesized Brønsted acidity of the support and residual H<sup>+</sup> protons on the catalyst after partial reduction. The catalyst was regenerated and tested for recyclability resulting in activity loss of ~12.5%, which was attributed to coke deposition.

**Supplementary Materials:** The following are available online at <http://www.mdpi.com/2073-4344/9/1/42/s1>, Figure S1: EDX mapping of Fresh Co/NaX, Figure S2: EDX spectrum of parent NaX, fresh Co/NaX, and spend Co/NaX, Table S1: Calculation of the Thiele modulus and effectiveness factor.

**Author Contributions:** J.C. and C.S. conducted the experiments. All authors analyzed the data and wrote the paper.

**Funding:** National Science Foundation NSF-CBET Award # 1705675.

**Acknowledgments:** M.C. thanks the National Science Foundation NSF-CBET Award # 1705675 for financial support of this work.

**Conflicts of Interest:** The authors declare no conflict of interest.

## References

1. Luo, N.; Cao, Y.; Li, J.; Guo, W.; Zhao, Z. Preparation of Ni<sub>2</sub>P/Zr-MCM-41 catalyst and its performance in the hydrodeoxygenation of Jatropha curcas oil. *J. Fuel Chem. Technol.* **2016**, *44*, 76–83. [[CrossRef](#)]
2. Yasir, M.; Azizan, M.T.; Ramli, A.; Ameen, M. Hydroprocessing of Crude Jatropha Oil Using Hierarchical Structured TiO<sub>2</sub> Nanocatalysts. *Procedia Eng.* **2016**, *148*, 275–281. [[CrossRef](#)]
3. Ameen, M.; Azizan, M.T.; Yusup, S.; Ramli, A.; Yasir, M. Catalytic hydrodeoxygenation of triglycerides: An approach to clean diesel fuel production. *Renew. Sustain. Energy Rev.* **2017**, *80*, 1072–1088. [[CrossRef](#)]
4. Demirbas, A. Diesel-like fuel from tallow by pyrolysis and supercritical water liquefaction. *Energy Sources Part A* **2009**, *31*, 824–830. [[CrossRef](#)]
5. Huber, G.W.; O'Connor, P.; Corma, A. Processing biomass in conventional oil refineries: Production of high quality diesel by hydrotreating vegetable oils in heavy vacuum oil mixtures. *Appl. Catal. A Gen.* **2007**, *329*, 120–129. [[CrossRef](#)]
6. Miao, C.; Marin-Flores, O.; Dong, T.; Gao, D.; Wang, Y.; Garcia-Pérez, M.; Chen, S. Hydrothermal Catalytic Deoxygenation of Fatty Acid and Bio-oil with in Situ H<sub>2</sub>. *ACS Sustain. Chem. Eng.* **2018**, *6*, 4521–4530. [[CrossRef](#)]
7. Crawford, J.M.; Carreon, M.A. Decarboxylation of Diunsaturated Linoleic Acid to Heptadecane over Zeolite Supported Pt/ZIF-67 Catalysts. *Ind. Eng. Chem. Res.* **2018**, *57*, 15991–15997. [[CrossRef](#)]
8. Snåre, M.; Kubičková, I.; Mäki-Arvela, P.; Chichova, D.; Eränen, K.; Murzin, D.Y. Catalytic deoxygenation of unsaturated renewable feedstocks for production of diesel fuel hydrocarbons. *Fuel* **2008**, *87*, 933–945. [[CrossRef](#)]
9. Besse, X.; Schuurman, Y.; Guilhaume, N. Hydrothermal conversion of linoleic acid and ethanol for biofuel production. *Appl. Catal. A Gen.* **2016**, *524*, 139–148. [[CrossRef](#)]
10. Kiméné, A.; Wojcieszak, R.; Paul, S.; Dumeignil, F. Catalytic decarboxylation of fatty acids to hydrocarbons over non-noble metal catalysts: The state of the art. *J. Chem. Technol. Biotechnol.* **2018**. [[CrossRef](#)]
11. Gosselink, R.W.; Hollak, S.A.W.; Chang, S.W.; Van Haveren, J.; De Jong, K.P.; Bitter, J.H.; Van Es, D.S. Reaction pathways for the deoxygenation of vegetable oils and related model compounds. *ChemSusChem* **2013**, *6*, 1576–1594. [[CrossRef](#)] [[PubMed](#)]
12. Hossain, M.Z.; Chowdhury, M.B.; Jhawar, A.K.; Xu, W.Z.; Charpentier, P.A. Continuous low pressure decarboxylation of fatty acids to fuel-range hydrocarbons with in situ hydrogen production. *Fuel* **2018**, *212*, 470–478. [[CrossRef](#)]
13. Ma, B.; Hu, J.; Wang, Y.; Zhao, C. Ni nanoparticles encapsulated into mesoporous single-crystalline HBEA: Application for drainage oil hydrodeoxygenation to diesel. *Green Chem.* **2015**, *17*, 4610–4617. [[CrossRef](#)]
14. Ma, B.; Yi, X.; Chen, L.; Zheng, A.; Zhao, C. Interconnected hierarchical HUSY zeolite-loaded Ni nano-particles probed for hydrodeoxygenation of fatty acids, fatty esters, and palm oil. *J. Mater. Chem. A* **2016**, *4*, 11330–11341. [[CrossRef](#)]
15. Ma, B.; Zhao, C. High-grade diesel production by hydrodeoxygenation of palm oil over a hierarchically structured Ni/HBEA catalyst. *Green Chem.* **2015**, *17*, 1692–1701. [[CrossRef](#)]
16. Li, W.; Gao, Y.; Yao, S.; Ma, D.; Yan, N. Effective deoxygenation of fatty acids over Ni(OAc)<sub>2</sub> in the absence of H<sub>2</sub> and solvent. *Green Chem.* **2015**, *17*, 4198–4205. [[CrossRef](#)]
17. Chen, N.; Gong, S.; Qian, E.W. Effect of reduction temperature of NiMoO<sub>3-x</sub>/SAPO-11 on its catalytic activity in hydrodeoxygenation of methyl laurate. *Appl. Catal. B Environ.* **2015**, *174–175*, 253–263. [[CrossRef](#)]

18. Wang, B.; Wang, D.; Guan, Y.; Xu, H.; Zhang, L.; Wu, P. Nickel/USY Catalyst Derived from a Layered Double Hydroxide/Zeolite Hybrid Structure with a High Hydrogenation Efficiency. *ChemCatChem* **2017**, *9*, 4552–4561. [[CrossRef](#)]
19. Weitkamp, J. Zeolites and catalysis. *Solid State Ion.* **2000**, *131*, 175–188. [[CrossRef](#)]
20. Vermeiren, W.; Gilson, J.P. Impact of zeolites on the petroleum and petrochemical industry. *Top. Catal.* **2009**, *52*, 1131–1161. [[CrossRef](#)]
21. Townsend, R.P.; Coker, E.N. Ion exchange in zeolites. *Stud. Surf. Sci. Catal.* **2001**, *137*, 467–524. [[CrossRef](#)]
22. Garcia, I.; Solache-Rios, M.; Bosch, P.; Bulbulian, S. Cobalt<sup>2+</sup> Ion Exchange with NaY. *J. Phys. Chem.* **1993**, *97*, 1249–1251. [[CrossRef](#)]
23. Song, W.; Zhao, C.; Lercher, J.A. Importance of size and distribution of Ni nanoparticles for the hydrodeoxygenation of microalgae oil. *Chem. Eur. J.* **2013**, *19*, 9833–9842. [[CrossRef](#)] [[PubMed](#)]
24. Breck, D.W. *Zeolite Molecular Sieves: Structure, Chemistry, and Use*, 1st ed.; Wiley: New York, NY, USA, 1974; ISBN 978-0471099857.
25. Suppes, G.J.; Dasari, M.A.; Doskocil, E.J.; Mankidy, P.J.; Goff, M.J. Transesterification of soybean oil with zeolite and metal catalysts. *Appl. Catal. A Gen.* **2004**, *257*, 213–223. [[CrossRef](#)]
26. Zhao, J.; Yu, W.; Chen, C.; Miao, H.; Ma, H.; Xu, J. Ni/NaX: A bifunctional efficient catalyst for selective hydrogenolysis of glycerol. *Catal. Lett.* **2010**, *134*, 184–189. [[CrossRef](#)]
27. Benaliouche, F.; Boucheffa, Y.; Ayrault, P.; Mignard, S.; Magnoux, P. NH<sub>3</sub>-TPD and FTIR spectroscopy of pyridine adsorption studies for characterization of Ag- and Cu-exchanged X zeolites. *Microporous Mesoporous Mater.* **2008**, *111*, 80–88. [[CrossRef](#)]
28. Ahmadi, M.; Macias, E.E.; Jasinski, J.B.; Ratnasamy, P.; Carreon, M.A. Decarboxylation and further transformation of oleic acid over bifunctional, Pt/SAPO-11 catalyst and Pt/chloride Al<sub>2</sub>O<sub>3</sub> catalysts. *J. Mol. Catal. A Chem.* **2014**, *386*, 14–19. [[CrossRef](#)]
29. Ahmadi, M.; Nambo, A.; Jasinski, J.B.; Ratnasamy, P.; Carreon, M.A. Decarboxylation of oleic acid over Pt catalysts supported on small-pore zeolites and hydrotalcite. *Catal. Sci. Technol.* **2015**, *5*, 380–388. [[CrossRef](#)]
30. Wang, Y.; Fang, Y.; He, T.; Hu, H.; Wu, J. Hydrodeoxygenation of dibenzofuran over noble metal supported on mesoporous zeolite. *Catal. Commun.* **2011**, *12*, 1201–1205. [[CrossRef](#)]
31. Hong, D.Y.; Miller, S.J.; Agrawal, P.K.; Jones, C.W. Hydrodeoxygenation and coupling of aqueous phenolics over bifunctional zeolite-supported metal catalysts. *Chem. Commun.* **2010**, *46*, 1038–1040. [[CrossRef](#)] [[PubMed](#)]
32. Wang, W.; Yang, Y.; Luo, H.; Hu, T.; Liu, W. Amorphous Co-Mo-B catalyst with high activity for the hydrodeoxygenation of bio-oil. *Catal. Commun.* **2011**, *12*, 436–440. [[CrossRef](#)]
33. Centeno, A.; Maggi, R.; Delmon, B. Use of noble metals in hydrodeoxygenation reactions. *Stud. Surf. Sci. Catal.* **1999**, *127*, 77–84. [[CrossRef](#)]
34. Bui, V.N.; Laurenti, D.; Delichère, P.; Geantet, C. Hydrodeoxygenation of guaiacol. Part II: Support effect for CoMoS catalysts on HDO activity and selectivity. *Appl. Catal. B* **2011**, *101*, 246–255. [[CrossRef](#)]
35. Valle, B.; Gayubo, A.G.; Alonso, A.; Aguayo, A.T.; Bilbao, J. Hydrothermally stable HZSM-5 zeolite catalysts for the transformation of crude bio-oil into hydrocarbons. *Appl. Catal. B Environ.* **2010**, *100*, 318–327. [[CrossRef](#)]
36. Zhang, H.; Lin, H.; Zheng, Y. The role of cobalt and nickel in deoxygenation of vegetable oils. *Appl. Catal. B Environ.* **2014**, *160–161*, 415–422. [[CrossRef](#)]
37. Lee, S.; Kim, H.; Choi, M. Controlled decationization of X zeolite: Mesopore generation within zeolite crystallites for bulky molecular adsorption and transformation. *J. Mater. Chem. A* **2013**, *1*, 12096–12102. [[CrossRef](#)]
38. Li, N.; Bi, Y.; Xia, X.; Chen, H.; Hu, J. Hydrodeoxygenation of Methyl Laurate over Ni Catalysts Supported on Hierarchical HZSM-5 Zeolite. *Catalysts* **2017**, *7*, 383. [[CrossRef](#)]
39. Tran, H.-L.; Kuo, M.-S.; Yang, W.-D.; Huang, Y.-C. Study on Modification of NaX Zeolites: The Cobalt (II)-Exchange Kinetics and Surface Property Changes under Thermal Treatment. *J. Chem.* **2016**, *2016*, 1–7. [[CrossRef](#)]
40. Yang, L.; Tate, K.L.; Jasinski, J.B.; Carreon, M.A. Decarboxylation of Oleic Acid to Heptadecane over Pt Supported on Zeolite 5A Beads. *ACS Catal.* **2015**, *5*, 6497–6502. [[CrossRef](#)]
41. Wei, Y.; Parmentier, T.E.; de Jong, K.P.; Zečević, J. Tailoring and visualizing the pore architecture of hierarchical zeolites. *Chem. Soc. Rev.* **2015**, *44*, 7234–7261. [[CrossRef](#)]

42. Díaz, E.; Ordóñez, S.; Vega, A.; Coca, J. Catalytic combustion of hexane over transition metal modified zeolites NaX and CaA. *Appl. Catal. B Environ.* **2005**, *56*, 313–322. [[CrossRef](#)]
43. Ilić, B.; Wettstein, S.G. A review of adsorbate and temperature-induced zeolite framework flexibility. *Microporous Mesoporous Mater.* **2017**, *239*, 221–234. [[CrossRef](#)]
44. Richardson, J.T.; Scates, R.; Twigg, M.V. X-ray diffraction study of nickel oxide reduction by hydrogen. *Appl. Catal. A Gen.* **2003**, *246*, 137–150. [[CrossRef](#)]
45. Starace, A.K.; Black, B.A.; Lee, D.D.; Palmiotti, E.C.; Orton, K.A.; Michener, W.E.; ten Dam, J.; Watson, M.J.; Beckham, G.T.; Magrini, K.A.; et al. Characterization and Catalytic Upgrading of Aqueous Stream Carbon from Catalytic Fast Pyrolysis of Biomass. *ACS Sustain. Chem. Eng.* **2017**, *5*, 11761–11769. [[CrossRef](#)]
46. Xing, S.; Lv, P.; Zhao, C.; Li, M.; Yang, L.; Wang, Z.; Chen, Y.; Liu, S. Solvent-free catalytic deoxygenation of oleic acid via nano-Ni/HZSM-5: Effect of reaction medium and coke characterization. *Fuel Process. Technol.* **2018**, *179*, 324–333. [[CrossRef](#)]
47. Król, M.; Mozgawa, W.; Jastrzębski, W. Theoretical and experimental study of ion-exchange process on zeolites from 5-1 structural group. *J. Porous Mater.* **2016**, *23*, 1–9. [[CrossRef](#)]
48. Busca, G. Acidity and basicity of zeolites: A fundamental approach. *Microporous Mesoporous Mater.* **2017**, *254*, 3–16. [[CrossRef](#)]
49. Regli, L.; Zecchina, A.; Vitillo, J.G.; Cocina, D.; Spoto, G.; Lamberti, C.; Lillerud, K.P.; Olsbye, U.; Bordiga, S. Hydrogen storage in Chabazite zeolite frameworks. *Phys. Chem. Chem. Phys.* **2005**, *7*, 3197–3203. [[CrossRef](#)]
50. Bauer, F.; Karge, H.G. *Characterization of Coke on Zeolites*; Karge, H.G., Weitkamp, J., Eds.; Springer: Berlin, Germany, 2007; ISBN 978-3-540-44825-9.
51. Triantafyllidis, K.; Lappas, A.; Stöcker, M. *The Role of Catalysis for the Sustainable Production of Bio-Fuels and Bio-Chemicals*, 1st ed.; Elsevier: Amsterdam, The Netherlands, 2013; ISBN 9780444563309.
52. Schreiber, M.W.; Rodriguez-Nino, D.; Gutierrez, O.Y.; Lercher, J.A. Hydrodeoxygenation of fatty acid esters catalyzed by Ni on nano-sized MFI type zeolites. *Catal. Sci. Technol.* **2016**, *6*, 7976–7984. [[CrossRef](#)]
53. Morgan, T.; Grubb, D.; Santillan-Jimenez, E.; Crocker, M. Conversion of triglycerides to hydrocarbons over supported metal catalysts. *Top. Catal.* **2010**, *53*, 820–829. [[CrossRef](#)]
54. Hermida, L.; Amani, H.; Abdullah, Z.A.; Mohamed, R.A. Deoxygenation of Palmitic Acid to Produce Diesel-like Hydrocarbons over Nickel Incorporated Cellular Foam Catalyst: A Kinetic Study. *J. Adv. Chem. Eng.* **2016**, *6*, 1–8. [[CrossRef](#)]
55. Fu, J.; Shi, F.; Thompson, L.T.; Lu, X.; Savage, P.E. Activated carbons for hydrothermal decarboxylation of fatty acids. *ACS Catal.* **2011**, *1*, 227–231. [[CrossRef](#)]
56. Wu, J.; Shi, J.; Fu, J.; Leidl, J.A.; Hou, Z.; Lu, X. Catalytic decarboxylation of fatty acids to aviation fuels over nickel supported on activated carbon. *Sci. Rep.* **2016**, *6*, 27820. [[CrossRef](#)]
57. Migliori, M.; Catizzone, E.; Aloise, A.; Bonura, G.; Gómez-Hortigüela, L.; Frusteri, L.; Cannilla, C.; Frusteri, F.; Giordano, G. New insights about coke deposition in methanol-to-DME reaction over MOR-, MFI- and FER-type zeolites. *J. Ind. Eng. Chem.* **2018**, *68*, 196–208. [[CrossRef](#)]
58. Guisnet, M.; Magnoux, P. Organic chemistry of coke formation. *Appl. Catal. A Gen.* **2001**, *212*, 83–96. [[CrossRef](#)]
59. Li, Y.; Zhang, C.; Liu, Y.; Hou, X.; Zhang, R.; Tang, X. Coke deposition on Ni/HZSM-5 in bio-oil hydrodeoxygenation processing. *Energy Fuels* **2015**, *29*, 1722–1728. [[CrossRef](#)]
60. Wilcox, J. *Carbon Capture*; Springer: New York, NY, USA, 2012; ISBN 9781461422150.
61. Zhang, J.; Zhao, C. Development of a Bimetallic Pd-Ni/HZSM-5 Catalyst for the Tandem Limonene Dehydrogenation and Fatty Acid Deoxygenation to Alkanes and Arenes for Use as Biojet Fuel. *ACS Catal.* **2016**, *6*, 4512–4525. [[CrossRef](#)]
62. Wu, G.; Zhang, N.; Dai, W.; Guan, N.; Li, L. Construction of Bifunctional Co/H-ZSM-5 Catalysts for the Hydrodeoxygenation of Stearic Acid to Diesel-Range Alkanes. *ChemSusChem* **2018**, *11*, 2179–2188. [[CrossRef](#)]
63. Shi, Y.; Xing, E.; Cao, Y.; Liu, M.; Wu, K.; Yang, M.; Wu, Y. Tailoring product distribution during upgrading of palmitic acid over bi-functional metal/zeolite catalysts. *Chem. Eng. Sci.* **2017**, *166*, 262–273. [[CrossRef](#)]
64. Soni, V.K.; Sharma, P.R.; Choudhary, G.; Pandey, S.; Sharma, R.K. Ni/Co-Natural Clay as Green Catalysts for Microalgae Oil to Diesel-Grade Hydrocarbons Conversion. *ACS Sustain. Chem. Eng.* **2017**, *5*, 5351–5359. [[CrossRef](#)]
65. Srifa, A.; Viriya-Empikul, N.; Assabumrungrat, S.; Faungnawakij, K. Catalytic behaviors of Ni/ $\gamma$ -Al<sub>2</sub>O<sub>3</sub> and Co/ $\gamma$ -Al<sub>2</sub>O<sub>3</sub> during the hydrodeoxygenation of palm oil. *Catal. Sci. Technol.* **2015**, *5*, 3693–3705. [[CrossRef](#)]

66. Liu, Q.; Bie, Y.; Qiu, S.; Zhang, Q.; Sainio, J.; Wang, T.; Ma, L.; Lehtonen, J. Hydrogenolysis of methyl heptanoate over Co based catalysts: Mediation of support property on activity and product distribution. *Appl. Catal. B Environ.* **2014**, *147*, 236–245. [[CrossRef](#)]
67. Ochoa-Hernández, C.; Yang, Y.; Pizarro, P.; de la Pena, V.A.; Coronado, J.M.; Serrano, D.P. Hydrocarbons production through hydrotreating of methyl esters over Ni and Co supported on SBA-15 and Al-SBA-15. *Catal. Today* **2013**, *210*, 81–88. [[CrossRef](#)]
68. Zhang, X.; Tang, D.; Zhang, M.; Yang, R. Synthesis of NaX zeolite: Influence of crystallization time, temperature and batch molar ratio  $\text{SiO}_2/\text{Al}_2\text{O}_3$  on the particulate properties of zeolite crystals. *Powder Technol.* **2013**, *235*, 322–328. [[CrossRef](#)]
69. Snåre, M.; Kubičková, I.; Mäki-Arvela, P.; Eränen, K.; Murzin, D.Y. Heterogeneous Catalytic Deoxygenation of Stearic Acid for Production of Biodiesel. *Ind. Eng. Chem. Res.* **2006**, *45*, 5708–5715. [[CrossRef](#)]
70. Froment, G.F.; Bischoff, K.B.; De Wilde, J. *Chemical Reactor Analysis and Design*, 3rd ed.; Wiley: New York, NY, USA, 2011; ISBN 978-0470565414.
71. Poling, B.E.; Prausnitz, J.M.; O'Connell, J.P. *The Properties of Gases and Liquids*, 5th ed.; McGraw-Hill: New York, NY, USA, 2001; ISBN 978-0070116825.



© 2019 by the authors. Licensee MDPI, Basel, Switzerland. This article is an open access article distributed under the terms and conditions of the Creative Commons Attribution (CC BY) license (<http://creativecommons.org/licenses/by/4.0/>).